MULTIRINGED IMPACT CRATERS ON VENUS FROM ARECIBO AND VENERA IMAGES. Jim S. Alexopoulos and William B. McKinnon. Dept. of Earth and Planetary Sciences and McDonnell Center for Space Sciences, Washington University, St. Louis, MO 63130; Valerie J. Hillgren, Lunar and Planetary Laboratory, University of Arizona, Tucson, AZ 85719.

We have analyzed peak-ring and multiringed impact basins on Venus in advance of and as a complement to Magellan data. Ringed basins are abundant on Venus, and thus serve as an important new data set that will further understanding of impact mechanisms in general and of the structural and rheological properties of the Venusian surface. Large ringed features of uncertain but clearly endogenic origin have also been identified.

Large multiringed impact craters on Venus were initially reported from Earth-based radar images. Arecibo [1,2,3,4] and Goldstone images [5] revealed circular and large quasi-circular structures of probable impact origin. Venera 15/16 radar images revealed 146 impact craters, 6 of which were classified as multiringed [6]. However, the morphologic characteristics of multiringed structures, and their surroundings, has led to differing interpretations of their origin (i.e., endogenic vs. exogenic) [7,8].

A reevaluation of high-resolution (1.5 to 2.5 km) Arecibo and Venera radar images reveals the presence of 18 multiringed and peak-ring impact craters on Venus (Table 1). The areal distribution of these features indicates no obvious spatial dependence. Peak-ring craters (or basins) are characterized by a broad, outer, radar-bright rim, and an inner bright ring defined by a concentric arrangement of numerous peaks (Fig. 1). The radar-bright returns of the inner and outer rings are mostly dominated by changes in average slopes of the topography. The ejecta patterns vary from regular (symmetric) to irregular (skewed due to oblique impact) and are characterized by radar returns that, due to the high incidence angles of the Arecibo radar, are dominated by roughness of the topography at the radar wavelength of 12.6 cm. Some of the peak-ring basins (~10%) show limited ejecta characteristics, as evidenced by their low radar albedo, which may indicate degradation (and age). Atmospheric and surficial processes, such as volcanism, may have attributed to this degradation. The interiors of most of the ringed craters are usually radar-dark. This is most likely attributed to their flooding by magma, which has since formed plains smooth relative to the radar wavelength. True multiringed basins, larger than peak-ring craters, are characterized by one prominent ring, up to 3 concentric rings (or partial rings), and exhibit Orientale-like morphologic similarities (i.e., Rook- and Cordillera-like rings) (Fig. 2). The two we have identified, Klenova and an unnamed structure (144- and 148-km-diameter, respectively), have radar returns similar to peak-ring craters, but exhibit a more subdued appearance. That is, the ejecta deposits are not as clearly defined, and the rings are partially obscured, relative to peak-ring craters. Their subdued appearance may be due to age, which has allowed obliterating processes (mainly volcanism) to alter their form.

The onset diameter for peak-ring craters, as revealed in a morphology-diameter histogram (Fig. 3), is ~40 km. This can be compared to peak-ring onset diameters on the other terrestrial planets: ~25, ~45, ~85, and ~140 km for Earth, Mars, Mercury, and the Moon, respectively [9]. Although the Venus transition is at a smaller diameter as expected for a higher gravity planet, the effective viscosity implied for peak-ring formation [e.g., 10] is less than that of the Moon and Mercury, and close to that of Mars, confirming that the scale dependence of the effective viscosity may dominate gravity in the formation of peak rings [11]. A plot of the ratio of the outer-rim-to-inner-ring diameter (D_{out}/D_{in}) against D_{out} (Fig. 4) reveals a relationship similar to that seen for Mercurian peak-ring basins [12]: the ratio is at first high, ~3, and then asymptotes with increasing diameter to the characteristic ratio of ~2. The relation $D_{out} = 2D_{in}$ (Fig. 5) is consistent with that observed for peak-rings on other terrestrial planets, but the two multiringed points fall off this trend and are closer to the $\sqrt{2}$ spacing canonical for this type of ringed structure.

Finite-element simulations of ring formation under Venus conditions have been carried out for the two largest multiringed structures here. The calculations are similar to [13], but a diabase crust of variable thickness is assumed to overly a dunite mantle, and the rheology is temperature (but not stress) dependent. Our preliminary findings are that thin-crust, moderate heat flow models (i.e, 10 km and 15 K/km [14]) do not produce rings (well defined tensional maxima in the radial stress); thicker crusts and heat flows closer to the global average (28 K/km) are necessary, although we have not yet produced a ring of the proper $\sqrt{2}$ spacing.

REFERENCES [1] Campbell, D.B. et al. (1990) GRL **17**, 1389-1392; [2] Burns, B.A. and Campbell, D.B. (1985) JGR **90**, 3037-3047; [3] Campbell, D.B. and Burns, B.A. (1980) JGR **85**, 8271-8281; [4] Thompson, T.W. and Saunders, R.S. (1986) EMP **36**, 167-185; [5] Schaber, G.G. and Boyce, J.M. (1977) In Impact and Explosion Cratering, 603-612; [6] Basilevsky, A.T. et al. (1987) JGR **92**, 12869-12901; [7] Schaber, G.G. et al. (1986) LPS XVII, 762-763; [8] Basilevsky, A.T. and Ivanov, B.A. (1990) GRL **17**, 175-178; [9] Pike, R.J (1983) JGR **88**, 2500-2504; [10] Melosh, H.J. (1989) Impact Cratering: A Geologic Process, 245pp; [11] Melosh, H.J.

and Gaffney, E.S. (1983) IGR 88, A830-A834; [12] McKinnon, W.B. (1981) Proc. LPSC 12A, 259-273; [13] Melosh, H.J. and Hillgren, V. (1987) LPS XVIII, 639-640; [14] Zuber, M.T. (1987) IGR 92, E541-E551.

Table 1

	NAME	lat.	long.	outer diameter (km)	inner diameter (km)
VENERA	RUSLANOVA	84.0	15.0	44.0	19.0
	KLENOVA	78.0	104.0	144.0	90.0
	CLEOPATRA	66.0	7.0	102.0	55.0
	BARSOVA	61.0	223.5	80.0	40.0
	WHARTON	55.5	62.0	54.0	21.0
	COCHRAN	52.0	143.0	104.0	48.0
	POTANINA	31.5	53.0	96.0	48.0
ARECIBO	-	33.7	288.6	77.3	36.0
	-	27.4	337.5	49.7	20.6
	-	18.2	326.5	57.2	26.1
	-	29.5	355.3	34.9	15.6
	-	25.4	25.2	81.9	43.8
	AKHMATOVA	61.3	308.0	41.5	13.2
	-	-44.4	271.1	49.8	14.3
	-	-10.7	11.8	38.4	11.4
	-	-45.6	335.5	40.7	14.8
	-	-52.4	329.6	48.9	20.6
	-	-55.7	321.7	148.4	95.3

Fig. 1

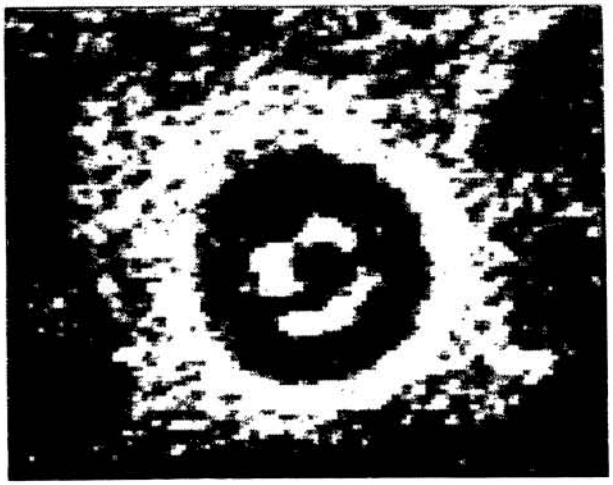

Fig. 2

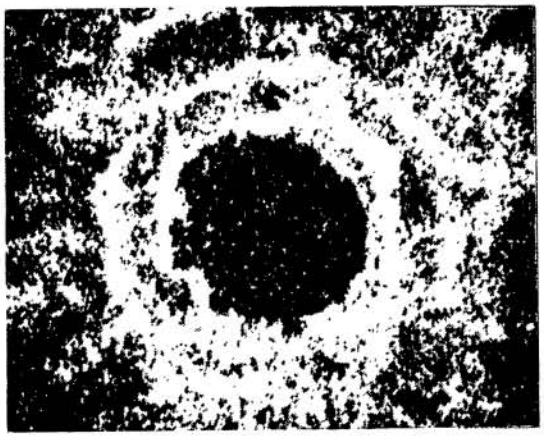

Fig. 3

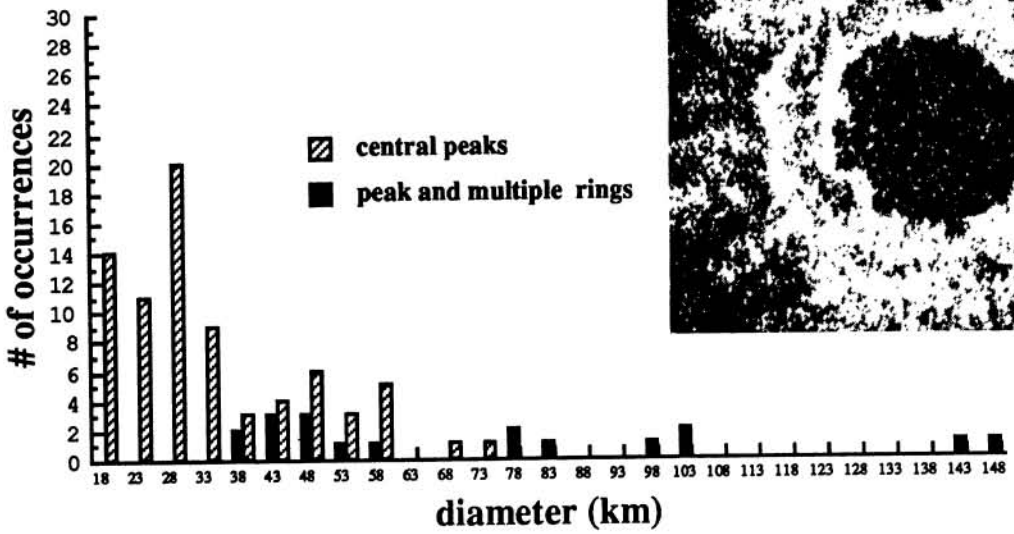

Fig. 4

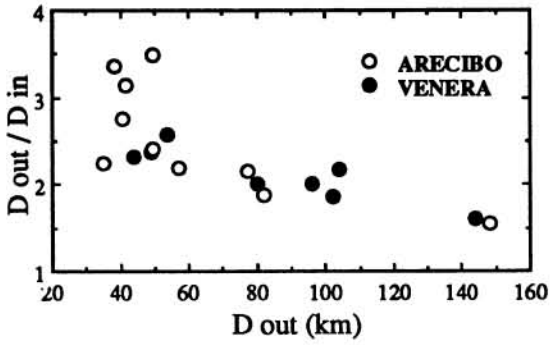

Fig. 5